Catal Lett (2012) 142:1251–1261
DOI 10.1007/s10562-012-0887-0

Direct Hydroxylation of Benzene to Phenol Over Mixed-Crystal Particles of Mesoporous VO_x/TiO_2 Catalyst Mixed-Crystal VO_x/TiO_2 for Benzene Hydroxylation

Dan Xu · Lihua Jia · Xiangfeng Guo

Received: 19 April 2012 / Accepted: 28 July 2012 / Published online: 14 August 2012

Abstract The influence of vanadium loading and calcination temperature on the catalytic performance of vanadia/TiO_2 (mixed-crystal) catalysts for the selective hydroxylation of benzene was investigated. A series of VO_x/TiO_2 catalysts were prepared using a range of vanadium loadings (2.27–9.06 wt %) and calcination temperatures of 450–650 °C. The samples were characterized using thermogravimetry–differential thermal analysis, N_2-adsorption, scanning electron microscopy, H_2 temperature-programmed reduction, X-ray diffraction, transmission electron microscopy, and X-ray photoelectron spectroscopy. It was found that vanadium exists as monomeric and polymeric VO_x and V_2O_5 crystal phases, depending on the amount of vanadium, accompanied by transformation of the TiO_2 carrier from anatase to rutile. The influence of temperature on the anatase to rutile transformation was strong, and only a little anatase was transformed to rutile at temperatures below 550 °C. When the temperature was raised to 650 °C, rutile became the main crystal phase. Monodisperse vanadia/TiO_2 (mainly anatase) catalysts are highly active in benzene hydroxylation to phenol, but aggregation of VO_x and crystalline V_2O_5 supported on a rutile carrier lowers the catalytic activity. In addition, the catalytic performances of the various catalysts in hydroxylation of benzene to phenol were investigated and possible reaction mechanisms are discussed.

D. Xu · L. Jia (✉)
College of Chemistry and Chemical Engineering of Qiqihar University, Qiqihaer 161006, China
e-mail: jlh29@163.com

X. Guo (✉)
Key Laboratory of Fine Chemicals (Qiqihar University), College of Heilongjiang Province, Qiqihaer 161006, China
e-mail: xfguo@163.com

Keywords Vanadium · Mixed-crystal · Mesoporous TiO_2 · Benzene · Hydroxylation · Phenol

1 Introduction

Phenol is an important industrial intermediate and is widely used for the production of phenolic resins, bisphenol A, epoxy resins, caprolactam, and aniline, for example. Phenol is mostly produced using the well-known cumene process. This process produces equimolar amounts of acetone as a by-product, and its use depends on the market price of acetone. The direct hydroxylation of benzene to phenol has therefore attracted much attention as an environmentally friendly and economically efficient process [1]. Recently, much effort has been devoted to finding a new synthetic route to phenol using a one-step process for the hydroxylation of benzene to phenol under mild conditions, for example, using nitrous oxide [2], molecular oxygen [3, 4], or hydrogen peroxide [5, 6]. The direct oxidation of benzene to phenol using H_2O_2 as an oxidant is widely accepted as a green process, with water as the only byproduct, and this may be one of the most useful processes in the future. However, finding higher activity catalysts, such as titanium–silica-based catalysts [7], Fe_2O_3/multiwalled carbon nanotubes [8], Fe^{3+}/MgO [9], $FeSO_4$/SiO_2 [10], Fe_3O_4/CMK-3 [11], Cu-MCM-41 [12], and CuAPO-11 [13], is challenging. Supported vanadia-based catalysts have been used in the hydroxylation of benzene to phenol [14–16]. Zhu et al. [17] have prepared VO_x/SBA-16 catalysts using an impregnation method; VO_x/SBA-16 with 7.3 wt % vanadium showed excellent activity for the hydroxylation of benzene with H_2O_2, and a selectivity of 97.5 %, with a phenol yield and turnover number of 13.8, and 32.4 %, respectively, in 4 h, were obtained. Feng et al.

[6] prepared a series of vanadium-containing hexagonal mesoporous silica (HMS) catalysts with different vanadium contents, using a coprecipitation method, for the direct hydroxylation of benzene to phenol with hydrogen peroxide, and a phenol yield of 11.1 % was obtained. Chen et al. [18] investigated the catalytic performance of $[(CH_3)_4N]_4$–$PMo_{11}VO_{40}$ for the hydroxylation of benzene and, with molecular oxygen as the oxidant, they found that 2,2,6,6-tetramethylpiperidine-1-oxyl (TEMPO) enhanced the catalytic performance, and the phenol yield reached 8.3 % with a selectivity of 95 % in 1 h. In our laboratory, V-HMS catalysts have been prepared and used for the direct hydroxylation of benzene to phenol using 30 % H_2O_2 as the oxidant; it was found that highly dispersed vanadium species could enhance the catalytic activity, and the best yield of phenol we obtained was 18.5 % with a selectivity of nearly 100 % [19]. It is still a major challenge to prepare catalysts with acceptable catalytic activity and selectivity for direct hydroxylation of benzene to phenol.

Vanadium supported on titania is commonly used as a catalyst for a number of industrially important reactions, including selective oxidation reactions of *o*-xylene to phthalic anhydride [20–22], ammoxidation of hydrocarbons [23, 24], and selective reduction of NO_x with NH_3 in the presence of O_2 [25–27]. The structural characteristics and catalytic activity and selectivity of vanadium/TiO_2 systems depend mainly on the method and conditions of preparation, such as the crystal structure of the titania, the vanadium loading, and the calcination temperature [28]. The dispersion of vanadia supported on TiO_2 is one of the main factors controlling catalytic performance [29]. The results of recent studies [30] indicate that a two-dimensional vanadia layer is the active phase in selective oxidation of hydrocarbons and it shows a higher activity and selectivity than bulk V_2O_5 crystallites. It is generally agreed that anatase-phase TiO_2 gives rise to epitaxial growth of vanadia, exposing the (010) plane monolayer, unlike rutile-phase TiO_2 [29]. It is well known that anatase TiO_2-supported catalysts undergo an anatase–rutile phase transformation at high temperatures, and a higher VO_x loading results in a higher surface density of nuclei for the phase transition from anatase to rutile, because replacement of Ti ions by vanadium ions, which are smaller, results in formation of a rutile solid-solution in which VO_x is dissolved [21, 31].

Although the structure of V_2O_5/TiO_2 and its catalytic properties have been extensively studied for some reactions, its direct use as a catalyst for the direct hydroxylation of benzene to phenol has received little attention. In this work, a series of TiO_2-supported VO_x catalysts with various amounts of vanadium oxide were synthesized using a hydrothermal synthesis method and used for hydroxylation of benzene to phenol. In particular, the structural evolution of VO_x/TiO_2 under the influence of thermal treatments, vanadium loading, and the interaction of vanadium oxide with titanium dioxide were studied using thermogravimetry–differential thermal analysis (TG–DTA), N_2 adsorption, scanning electron microscopy (SEM), transmission electron microscopy (TEM), X-ray diffraction (XRD), H_2 temperature-programmed reduction (H_2-TPR), and X-ray photoelectron spectroscopy (XPS). The results indicated that composites with different vanadium loadings, and produced using different calcination temperatures, had different crystalline phases, and there was a strong interaction between the carrier and the vanadium species. The relationship between the catalyst structure and catalytic properties are discussed. The VO_x/TiO_2 catalyst calcined at 550 °C and with a vanadium loading of 4.30 wt % was a mixture of anatase and rutile (12.6 wt %), and exhibited excellent catalytic properties in the hydroxylation of benzene to phenol at 60 °C with a high phenol yield of around 23.8 %, and a phenol selectivity of about 85 %. A possible mechanism for the hydroxylation of benzene to phenol and the catalytic performance are discussed.

2 Experimental

2.1 Catalyst Preparation

The VO_x/TiO_2 catalyst was prepared by hydrothermal synthesis using laurylamine (DDA) (98 %, SCRC, Shanghai, China) as a template, tetrabutyl titanate (TBOT, 98 %, SCRCs), isopropanol (>99 %, SCRC), and ammonium metavanadate (NH_4VO_3, ≥99.0 %, SCRC) as precursors. In a typical synthesis, about 2.5 g of DDA, 21 g of absolute ethanol, 36 g of deionized water, and a given amount of NH_4VO_3 were first mixed. After vigorous stirring at 30 °C for 30 min, a mixture of 17 g of TBOT and 6.0 g of isopropanol was slowly added under vigorous stirring; a buff sediment was immediately formed. The molar ratio of the mixture was 1.0 TiO_2:*x* NH_4VO_3:0.27 DDA:9.0 ethanol:2.0 isopropanol:40 H_2O. After stirring for 24 h, the mixture was aged without stirring at 30 °C for 24 h. The resulting mixture was filtered and the precipitate was washed once with deionized water (200 mL) and then five times with absolute ethanol (50 mL). The precipitate was dried at 80 °C overnight and calcined at different temperatures (450–650 °C), with a heating rate of 2 °C min^{-1}, for 6 h to remove the organic species. The obtained sample was denoted by TiV(*T*)-*n* (*T* represents the calcination temperature, $T = 450$, 500, 550, 600, 650 °C, and *n* represents the weight percentage of vanadium, $n = 2.27$, 3.36, 4.30, 6.93, and 9.06 wt %).

2.2 Catalysts Characterization

Thermogravimetric analysis (TG/DTA) was carried out in air atmosphere with a Mettler TC-10 thermo balance (Diamond TG/DTA, Perkin Elmer) from room temperature to 900 °C at a heating rate of 20 °C min^{-1}. Powder X-ray diffraction (XRD) patterns were recorded on a Germany Bruker D8 Advance diffractometer using Cu K*a* radiation ($\lambda = 1.5418$ Å). Nitrogen adsorption isotherms were measured at −196 °C on Quantachrome NOVA2000e. The samples were degassed at 300 °C for 3 h before the measurement under vacuum (10^{-3} Torr). The specific surface areas were determined according to the Brunauer–Emmett–Teller (BET) method in the relative pressure range of 0.05–0.3. The pore volumes were calculated from the nitrogen volume adsorbed at the relative pressure of 0.99. Pore size distribution (PSD) curve was derived from the Barrett–Joyner–Halenda (BJH) method using the adsorption branch. The pore size was estimated from the maximum position of the BJH–PSD curve. Morphology of the samples was observed with scanning electron microscope (SEM) on a Rigaku S-4300 spectrometer coupled with an energy dispersive spectroscopy (EDS). The microscopic feature of the samples was observed with transmission electron microscope (TEM) on a Rigaku H-7650 scan-transmission electron microscope with 100 kV. H_2-TPR measurement was performed in a quartz tubular microreactor on Quantachrome Chem-BET3000. Catalyst sample (50 mg) was placed in the reactor and subjected to a gas flow of pure Ar (120 mL/min) at 500 °C for 1 h, followed by cooling down to 50 °C in pure Ar flow. After that, the sample was heated in H_2–Ar flow (80 mL/min, containing 10 mol% H_2/Ar) from 50 to 800 °C at the rate of 10 °C min^{-1}. The amount of H_2-consumption during the heating for reduction was measured by a thermal conductivity detector (TCD). The surface chemical composition of the catalysts was determined by X-ray photoelectron spectroscopy (XPS) on a VG ESCALAB 250 spectrometer (Thermo Electron, UK), using a non-monochromatized Al K*a* X-ray source (1486 eV).

2.3 Catalytic Test and Analytic Procedure

The liquid-phase oxidation of benzene to phenol was carried out in a three-necked round-bottomed flask (50 mL) with a magnetic stirrer. In a typical reaction, the required amount of calcined catalyst powder was fully dispersed in 5.0 mL acetonitrile (CH_3CN, A. R.) followed by the addition of 2.3 g (0.03 mol) benzene (A.R.). After stabilization of the temperature, the required amount of H_2O_2 (30 wt % in H_2O, A.R.) was added in one lot and the benzene hydroxylation process was kept going with magnetic stirring for a period of time. After that, the reaction solution was cooled to ambient temperature, and the solid catalyst was separated by centrifugation. The liquid product was analyzed using a gas chromatograph equipped with a flame ionization detector [Cotrun GC9800(N)] and fitted with a KB-17 (30 m × 0.25 mm × 0.25 μm) capillary column. The temperatures of the sample injector and detector were 250 and 280 °C, respectively. The temperature program for the product analysis was as follows: the initial temperature, 50 °C, was maintained for 4 min, and increased at a rate of 15 °C min^{-1} to the final temperature of 200 °C; methylbenzene was used as the internal standard. Under the employ conditions, only benzoquinone was detected as the by-product. Conversion and selectivity were calculated by comparing with relative area of each of authentic samples, which is proportional to the concentration of the substance.

$$\text{Yield of phenol} = \text{mol phenol}/(\text{mol initial benzene}).$$

$$\text{Conversion of benzene} = \text{mol reacted benzene} / (\text{mol initial benzene}).$$

$$\text{Selective of phenol} = \text{yield of phenol} / (\text{conversion of benzene}).$$

3 Results and Discussion

3.1 TG–DTA, XRD, Pore Structure, and Microstructure Analysis

The TG analysis results for the TiV-4.30 precursor are shown in Fig. 1. In the TG curve, the sample showed a total weight loss of ~47 % on heating to 900 °C. The first effect, below 180 °C, was attributed to the release of physically absorbed water, the second was attributed to desorption and decomposition of the DDA template between 200 and 550 °C [32, 33], and the third effect represents the transformation of anatase to the rutile phase from 550 to 850 °C. The DTA curve exhibited a large exothermic peak corresponding to desorption and decomposition of surfactants and the crystallization of mesoporous TiO_2. There was no mass loss from the composite above 850 °C.

The sample microstructures were examined using low-angle XRD patterns of the TiV(*T*)-4.30 catalysts for different calcination temperatures, as shown in Fig. 2a. All the catalysts contained a low single-angle diffraction peak, characteristic of mesoporous materials, corresponding to the (100) basal line. The intensity and degree order of the patterns decreased slightly with increasing temperature. The wide-angle XRD patterns are shown in Fig. 2b. It is obvious that the main peaks at $2\theta = 25.5$, 37.9, 48.1, 54.1, and 62.6° were the (101), (004), (200), (105), and (204) diffraction peaks of anatase-phase TiO_2 (JCPDS 21-1272),

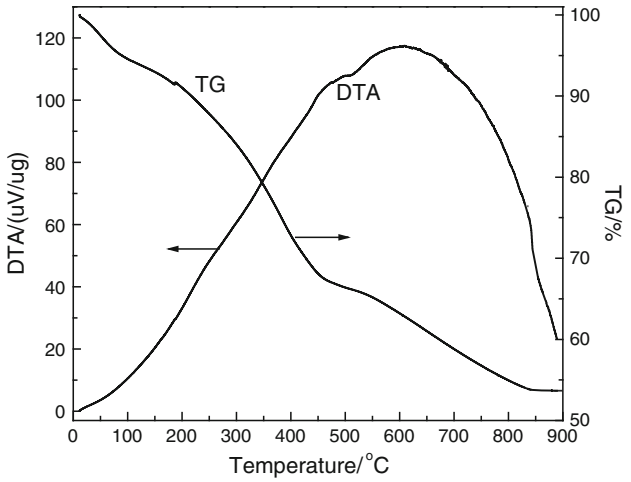

Fig. 1 TG–DTA curves recorded for the TiV-4.30 catalyst

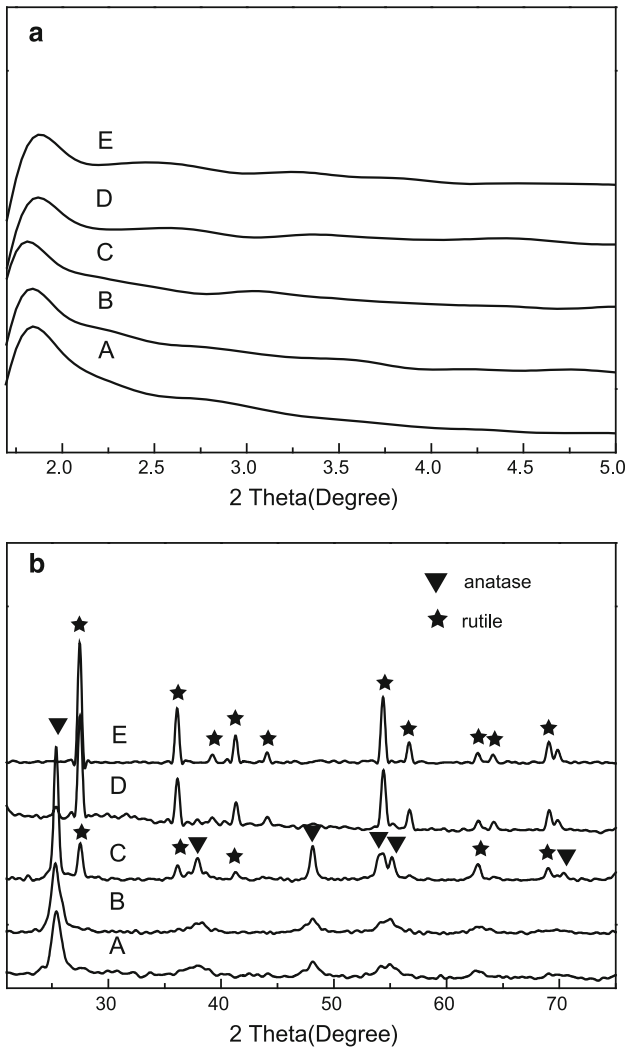

Fig. 2 XRD patterns (**a** low angle; **b** wide angle) of TiV(*T*)-4.30 catalysts with different calcination temperatures: *A* 450 °C, *B* 500 °C, *C* 550 °C, *D* 600 °C, and *E* 650 °C

for calcination temperature 450, 500, and 550 °C [34, 35]. A very weak peak appeared at $2\theta = 27.4°$, which belonged to the (110) diffraction peak of the rutile phase at 550 °C, but the main diffraction peaks correspond to the anatase phase. When the temperature was increased to 600 or 650 °C, the catalyst was transformed into almost pure rutile TiO_2, because the anatase phase, which is a metastable phase, was transformed to the stable rutile phase at higher temperatures [48]. This indicated that higher temperatures were favorable for phase transformation [21].

The wide-angle XRD patterns of catalysts with different vanadium contents (calcined at 550 °C) are shown in Fig. 3a. It was found that the added V_2O_5 promotes the anatase–rutile phase transformation in TiO_2-supported catalyst powders. Without vanadium doping, the sample was mostly in the anatase phase. As the vanadium loading increased from 2.27 to 9.06 wt %, the crystalline phase changed significantly. When the powder mixture contained a small amount of vanadium, there was a small amount of the rutile phase. The relationship between percentage composition of rutile and the vanadium loading is shown in Fig. 3b. When the vanadium loading was 9.06 wt %, the fraction of rutile was 92.4 wt %, which indicated that the loading of the vanadia species could dramatically accelerate transformation of anatase to rutile. In addition, the diffraction peaks at $2\theta = 20.23$, 26.08, and 31.03° correspond to the formation of bulk V_2O_5 on the composite surfaces. All of these results are in agreement with the literature [17, 36].

N_2-physisorption isotherms of all the TiV(*T*)-4.30 samples, calcined at various temperatures, are shown in Fig. 4a. All the N_2-physisorption isotherms were classical type IV, with a typical H_2 hysteresis loop between the adsorption and the desorption curves, indicating the existence of pores with narrow entrances and large cavities [37, 38]. When the calcination temperature was 650 °C, the hysteresis loop of a given sample shifted to the high pressure P/P_0 range and its slope became gentler; this may be a result of crystallization of the sample, subsequent crystal growth, and collapse of the mesoporous structure [32]. The pore size distribution of the TiV(*T*)-4.30 samples are shown in Fig. 4b, estimated using the Barrett–Joyner–Halenda (BJH) method from the desorption branches. It was obviously that all the samples had narrow pore size distributions (3–5 nm) and uniform pore structures, and the pore size distribution became narrower with increasing calcination temperature, indicating that higher temperatures caused structural changes in the catalyst; this is consistent with the XRD analysis.

The detailed structural parameters of the TiV(*T*)-4.30 catalysts, calcined at various temperatures, are shown in Table 1. As the calcination temperature increased, the surface areas and average pore sizes of the materials increased. The largest Brunauer–Emmett–Teller (BET)

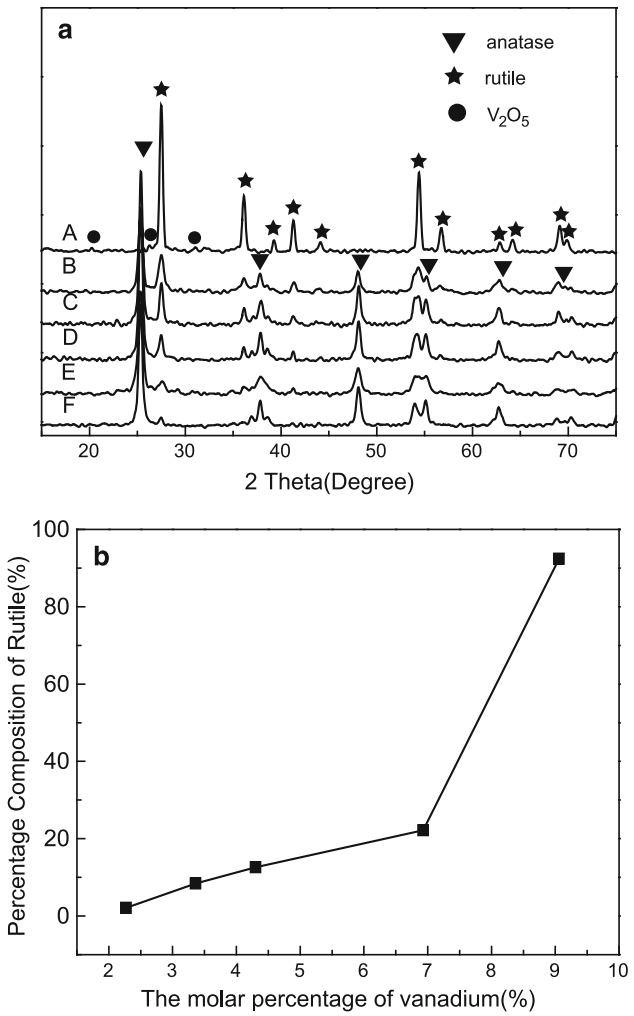

Fig. 3 XRD patterns (**a**) and the percentage compositions of rutile and vanadium (**b**) of catalysts with different vanadium contents and calcination temperature of 550 °C: *A* TiV-9.06, *B* TiV-6.91, *C* TiV-4.30, *D* TiV-3.34, *E* TiV-2.27, and *F* TiO_2

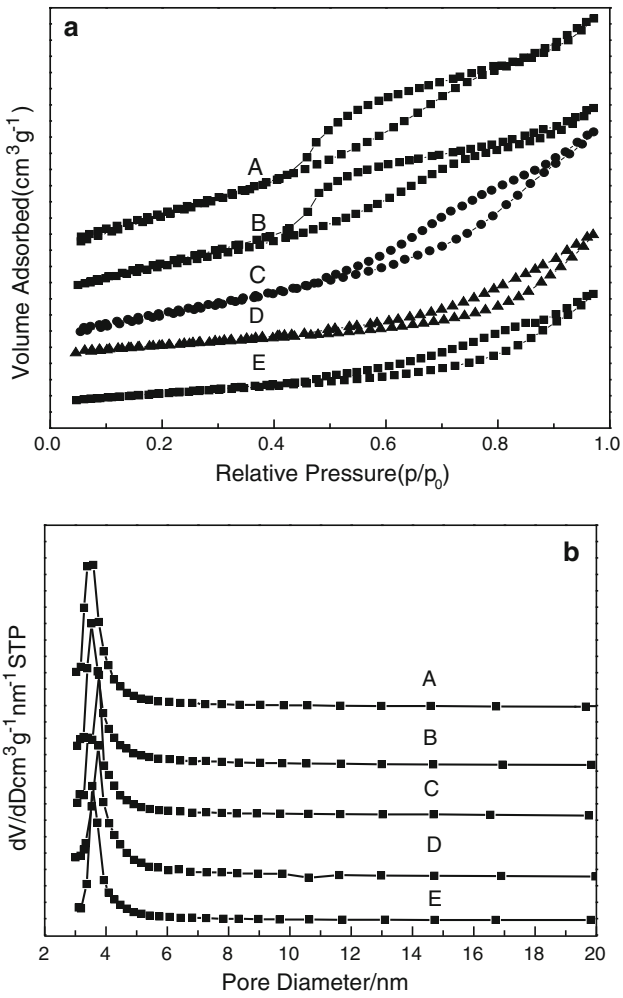

Fig. 4 N_2 adsorption–desorption isotherms (**a**) and pore size distributions (**b**) of TiV(*T*)-30 catalysts for different calcination temperatures: *A* 450 °C, *B* 500 °C, *C* 550 °C, *D* 600 °C, and *E* 650 °C

specific area, 83 m^2/g, was obtained for the sample calcined at 550 °C; the pore volume and pore size were 0.11 cm^3/g and 3.8 nm, respectively. However, the size of the particles increased from 16 to 54 nm for a calcination temperature of 650 °C, and the surface area and pore volume were 11 m^2/g and 0.016 cm^3/g, respectively, indicating that the sample crystal type changed at higher calcination temperatures [37]. These results are in agreement with the XRD analysis.

The physicochemical properties of samples with different vanadium loadings, calcined at 550 °C, are listed in Table 2. It can be seen that impregnation with vanadium species increased from 0 to 4.30 wt %, there was a notable increase of the sample surface area from 25 to 83 m^2/g, and the grain size decreased from 24 to 16 nm. The reason may be that vanadium species hinder crystalloid growth [39]. With the loading amount of vanadium species reached 9.06 wt %, there were negligible decreases in the specific area, pore volume, and pore diameter of the sample, but the grain size increased from 16 to 29 nm, which may be caused by the extra vanadium and the carrier TiO_2 forming a $V_xTi_{1-x}O_2$ rutile-phase solid-solution [21].

Figure 5 shows the SEM and TEM images of the TiV(550)-4.30 sample. The particles were spherical and the crystal sizes were about 15 nm, close to the XRD result (16.4 nm). Magnified TEM images of the material are shown in Fig. 5b, c; it can be observed that discernible pores were present at the surface of the mesoporous TiV(550)-4.30 material, and the particle size was around 15 nm, corresponding to the SEM image results. The pore properties were investigated using high-resolution TEM (Fig. 5d). The pores can be seen as black spots, with an ordered wormhole-like mesoporous structure on the sample surface [37]. In large areas, the *d*-spacings of these nanocrystals were 0.35 and 0.32 nm, related to (101) plane anatase and (110) plane rutile, respectively [40, 41].

Table 1 Structural parameters of TiV(*T*)-4.30 samples calcined at various temperatures

Catalyst	2θ (°)	d_{101}/d_{110} (nm)	S^a_{BET} (m^2/g)	V^b (cm^3/g)	D^c(nm)	Dcry.[d] (nm)
TiV(450)-4.30	25.35	0.35	60	0.10	3.7	14.4
TiV(500)-4.30	25.34	0.35	74	0.10	3.8	14.9
TiV(550)-4.30	25.33	0.35	83	0.11	3.9	16.4
TiV(600)-4.30	27.46	0.32	39	0.09	3.9	45.6
TiV(650)-4.30	27.46	0.32	11	0.02	4.1	54.6

[a] Surface area, derived from BET equation

[b] Pore volume, obtained from the volume of nitrogen adsorbed at the relative pressure of 0.99

[c] Pore size, derived from BJH method using adsorption branch

[d] Dcry., crystal particle size derived from XRD

Table 2 Structural parameters of catalysts with different vanadium contents at 550 °C

Catalyst	2θ (°)	d_{101} (nm)	S_{BET} (m^2/g)	V (cm^3/g)	D (nm)	Dcry. (nm)
TiV(550)-9.06	27.52	0.33	31	0.07	3.1	29.6
TiV(550)-6.91	25.30	0.35	48	0.09	3.3	20.7
TiV(550)-4.30	25.33	0.35	83	0.11	3.9	16.4
TiV(550)-3.34	25.41	0.35	27	0.06	3.8	23.1
TiV(550)-2.27	25.36	0.35	27	0.06	3.9	23.9
TiV(550)-0	25.29	0.33	25	0.05	3.7	24.1

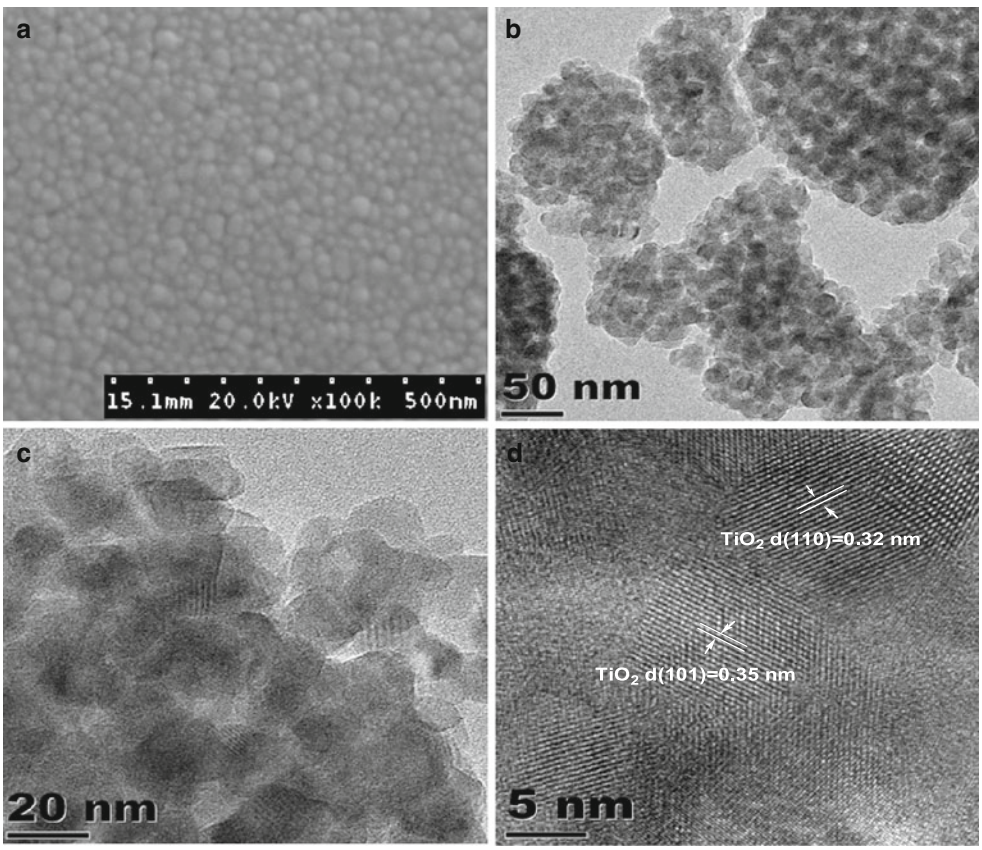

Fig. 5 SEM and TEM images of TiV(550)-4.30 sample

3.2 Reducibility and XPS Analysis

To gain a better understanding of the high efficiency of the active sites, the H_2-TPR profiles of samples with different vanadium loadings, calcined at 550 °C, were obtained (Fig. 6). The pure TiO_2 had no reduction peak, and the pure V_2O_5 species exhibited two reduction peaks in the temperature range 600–800 °C, corresponding to the consecutive processes $V_2O_5 \rightarrow 1/3V_6O_{13} \rightarrow 2VO_2$; V_6O_{13}, which was formed (reduction peak at 660 °C) as an intermediate product, was not stable and was easily reduced to VO_2 [42]. It was found that the reduction temperatures of the VO_x/TiO_2 catalysts depended on the vanadium loadings. The reduction peaks of the VO_x species shifted to lower temperatures for vanadium loadings less than 9.06 wt %), and the TPR curves exhibited only one major reduction peak, at around 550 °C, attributed to the reduction of monodisperse vanadium species (VO_x) on the carrier TiO_2 surface. The shift of the maximum of the H_2 consumption peak to a lower temperature suggested that there may be strong interactions between the VO_x species and the carrier [43]; the formation of V–O–Ti bonds with significantly higher reducibility [44] and the valence of the vanadium species will be further discussed in the context of the XPS results. The monodisperse vanadium species was the main active species in the selective oxidation reaction. As the vanadium loading increased to 9.06 wt %, other reduction peaks appeared at 670 °C, corresponding to the first peak of crystalline V_2O_5, attributed to reduction of large particles of aggregated VO_x species or crystalline V_2O_5 species on the TiO_2 surface [45]; this indicated that the isolated VO_x aggregates and crystallized V_2O_5 formed with increasing vanadium loading. The results are close to those obtained in the XRD analysis.

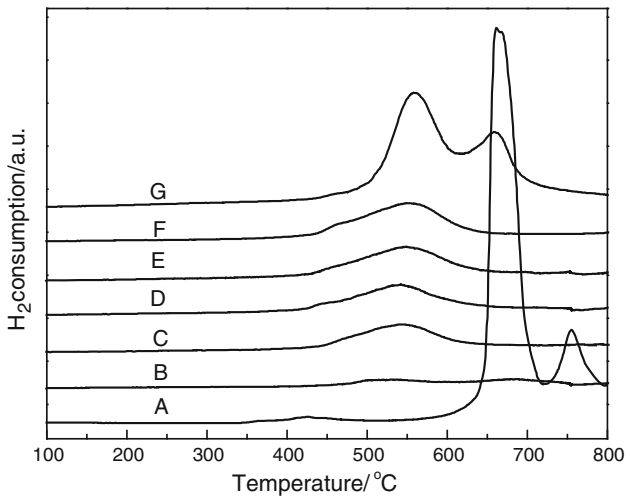

Fig. 6 H_2–TPR curves of catalysts with different vanadium contents and calcination temperature of 550 °C: *A* V_2O_5, *B* TiV-9.06, *C* TiV-6.91, *D* TiV-4.30, *E* TiV-3.34, *F* TiV-2,27, and *G* TiO_2

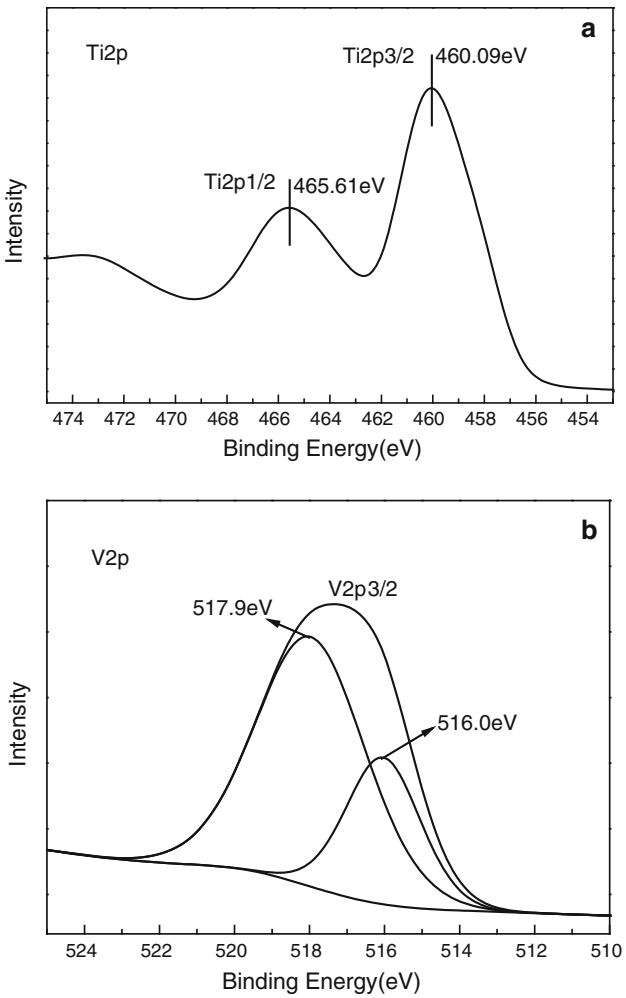

Fig. 7 XPS spectra of **a** Ti2p and **b** V2p of TiV(550)-4.30 catalyst

XPS is a good tool for investigating the surface element compositions and metal oxidation states of solid materials. The XPS results for the TiV(550)-4.30 catalyst are shown in Fig. 7. As shown in Fig. 7a, two main peaks, at 465.6 and 460.0 eV, were observed in the Ti2p spectrum. These peaks are related to the Ti2p1/2 and Ti2p3/2 states of TiO_2 and show the +4 valence state of Ti cations in TiO_2 [46]. The XPS spectrum of V2p3/2 is shown in Fig. 7b; the binding energies of 517.9 and 516.0 eV were attributed to V^{5+} and V^{4+}, respectively, in the TiV(550)-4.30 sample [47, 48]. It was considered that the vanadium species had mixed +4 and +5 valence states on the catalyst surface. As previously reported, calcination at high temperature resulted in a specific reaction between dispersed V^{5+} ions and the matrix, resulting in the formation of V^{4+} [42].

3.3 Catalytic Activity Test

The activities of the TiV(*T*)-4.30 catalysts calcined at various temperatures were assessed in the liquid-phase

hydroxylation of benzene with H_2O_2 as the oxidant; the results are plotted in Fig. 8. It is obvious that the yield of phenol initially increased with increasing calcination temperature. The highest activity for the hydroxylation of benzene was obtained at a temperature of 550 °C; the phenol yield was 23.7 %. As the temperature continued to increase, there was a notable decrease in the phenol yield, mostly because the samples were mainly rutile phase with a dramatic decrease in the specific surface area. In addition, the available amount of monodisperse vanadium on the TiO_2 support decreased. These data indicated that a calcination temperature of 550 °C was the most favorable; the amount of rutile phase in the mixed-crystal TiO_2 carrier was 12.6 wt %, which suggested that a mixed-crystal TiO_2 carrier with a low rutile content was most conductive to the reaction.

Figure 9 shows the influences of catalysts with different amounts of vanadium species and a calcination temperature of 550 °C on the hydroxylation of benzene. It can be seen from the figure that the yield and selectivity of phenol, and the conversion rate of benzene, initially increased with vanadium species loading, and the maximum phenol yield, 23.7 %, was obtained when the vanadium loadings was 4.30 wt %. The yield of phenol decreased slightly with further increases in the vanadium species loading, because the active VO_x components would aggregate and easily form a $V_xTi_{1-x}O_2$ rutile-phase solid-solution with TiO_2. The formation of a solid solution would have an unfavorable effect on the total catalytic activity and on the oxidation product. A vanadium loading of 4.3 wt % was therefore considered to be suitable for hydroxylation of benzene to phenol.

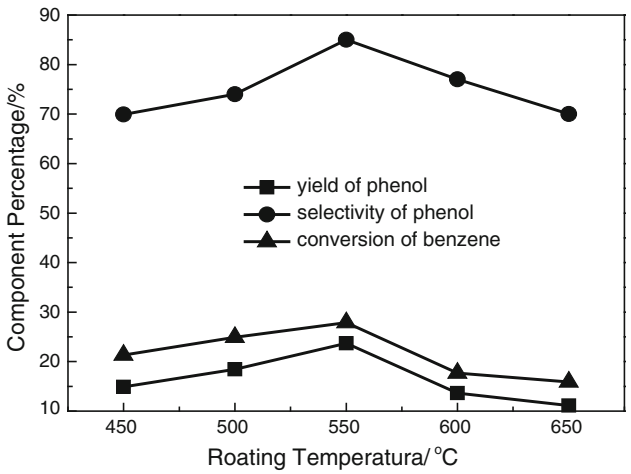

Fig. 8 Effects of TiV(*T*)-4.30 catalysts calcined at various temperatures on hydroxylation of benzene. Benzene (0.03 mol): H_2O_2 = 1:2, 0.18 g TiV(*T*)-4.30, 5 mL acetonitrile, T = 60 °C, *t* = 5 h

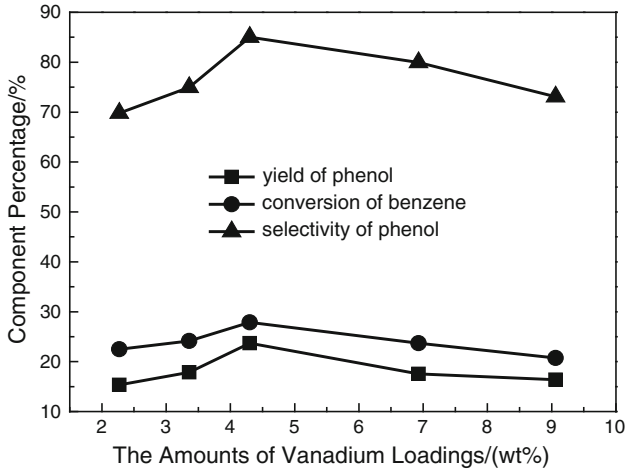

Fig. 9 Effects of catalysts with different vanadium contents, calcined at 550 °C, on hydroxylation of benzene. Benzene (0.03 mol): H_2O_2 = 1:2, 0.18 g TiV(550)-*n*, 5 mL acetonitrile, T = 60 °C, *t* = 5 h

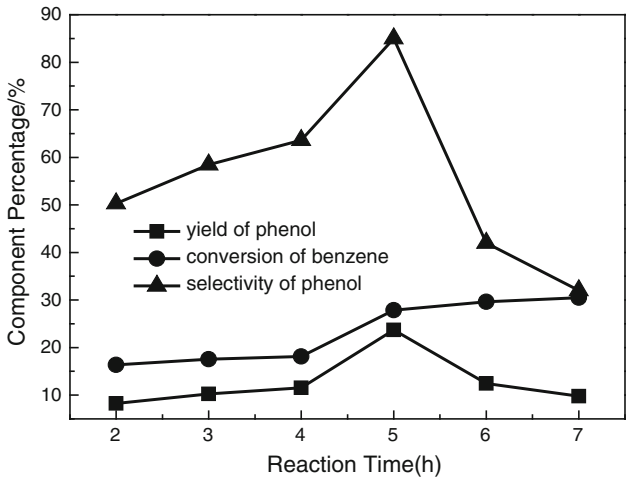

Fig. 10 Effects of reaction time on hydroxylation of benzene. Benzene (0.03 mol):H_2O_2 = 1:2, 0.18 g TiV(550)-4.30, 5 mL acetonitrile, T = 60 °C

The effects of the various reaction conditions including reaction temperature, reaction time and the amount of the catalyst on the yield of phenol were also investigated over TiV(550)-4.30 catalyst for hydroxylation of benzene. The results are presented in Figs. 10, 11, and 12. Figure 10 shows a plot of benzene conversion and phenol selectivity as a function of reaction time. It indicates that higher benzene conversions may be achieved with prolonging reaction time. However, prolonging reaction time results in a drop in selectivity for phenol, due to the further oxidation of phenol. The conversion of benzene reached 28 % with a high selectivity of 85 % at 5 h. The effect of reaction temperature on benzene hydroxylation is shown in Fig. 11. When the

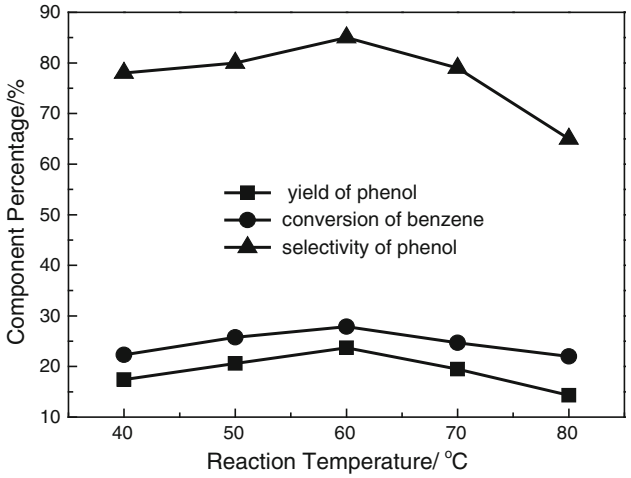

Fig. 11 Effects of reaction temperature on hydroxylation of benzene. Benzene (0.03 mol): H_2O_2 = 1:2, 0.18 g TiV(550)-4.30, 5 mL acetonitrile, t = 5 h

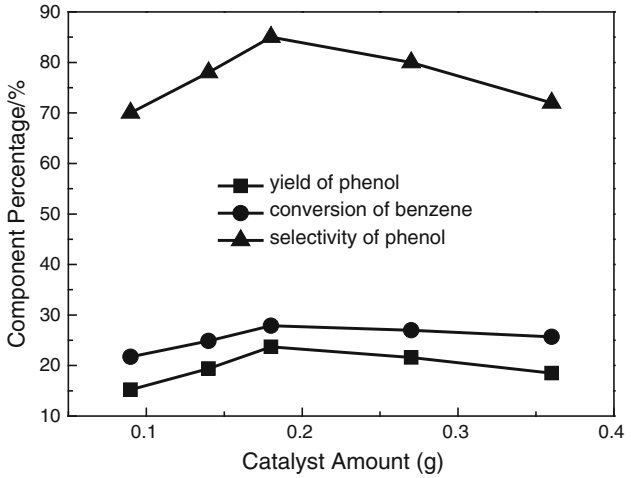

Fig. 12 Effects of TiV(550)-4.30 catalyst amount on hydroxylation of benzene. Benzene (0.03 mol): H_2O_2 = 1:2, 5 mL acetonitrile, T = 60 °C, t = 5 h

reaction temperature was raised to 60 °C, the phenol yield was 23.7 % in the best case. And the conversion of benzene decreased at higher temperatures because of the spontaneous decomposition of H_2O_2 to O_2 and H_2O at high temperatures and that some H_2O_2 vanish without being involved in the catalysis. As for the selectivity, it follows a trend to descend with the increase of reaction temperature. This might be due to the further oxidation of phenol at high temperatures. As shown in Fig. 12, the dependence on the TiV(550)-4.30 amount was investigated. With an amount of catalyst increased from 0.09 to 0.18 g leads to the yield of phenol from 15.2 to 23.7 % because of the formation of a large amount of vanadium active species. Further increase in the amount of TiV(550)-4.30 could not result in a higher yield of phenol, meanwhile the selectivity of phenol has gradually decreased, this could be attributed to the further oxidation of phenol by excess vanadium active species.

From all the above results, it could get the optimum reaction conditions: 0.18 g TiV(550)-4.30, reaction temperature 60 °C, reaction time 5 h, and a fixed amount of solvent (5 mL), benzene (0.03 mol) and 30 wt % H_2O_2 (0.06 mol). And the highest yield of phenol was 23.7 %, with the phenol selectivity of about 85 %".

According to the structural characterization of catalysts and the results shown in Figs. 8, 9, 10, 11, and 12, the activity of the catalyst greatly depended on the decentralized state of vanadium and the crystal phase of the carrier. Vanadium had two valences (+4 and +5) on the sample surface. As previously reported, the essential role of anatase TiO_2 is to enable formation of a VO_x monolayer to provide essentially complete dispersion of the vanadium on a support, with an adequate but not excessive surface area [43]. The condition for stability of the supported oxides is that the two cations should have similar electronegativities; Ti–O (anatase) and V–O bonds have similar polarities, but rutile is not so suitable [37]. In this study, it was clearly shown that the catalyst had high activity when it contained a small amount (12.6 wt %) of rutile phase, so maybe a small number of V^{4+} ions migrated toward the TiO_2 matrix and became magnetically isolated by forming a $V_xTi_{1-x}O_2$ rutile-phase solid-solution structure [30, 42], but the mixed-valence V^{4+} and V^{5+} were the active centers and were highly dispersed on the mixed-crystal surface. Too high a vanadium content would cause aggregation on the catalyst surface, and formation of a $V_xTi_{1-x}O_2$ rutile-phase solid-solution with TiO_2 would be easy. This change in the catalyst structure would decrease the catalytic activity. So, too high or too low vanadium contents were disadvantageous to the reaction, and the TiV(550)-4.30 catalyst exhibited excellent catalytic performance for the hydroxylation of benzene to phenol.

In hydroxylation reactions of aromatic compounds using H_2O_2 as the oxidant, different peroxide intermediates can be formed with various metal oxides, and the metal and the H_2O_2 can form a metal-peroxo transition state [49]. In this study, a vanadium(+4) species first interacted with H_2O_2 and was rapidly transformed into a relatively stable vanadium(+5) species [16, 50]. Then the vanadium(+5) species and H_2O_2 formed a vanadium(+5)-peroxo intermediate species, which combined with benzene, after losing a water molecule, to complete the hydroxylation reaction[51–54]. A possible reaction mechanism is shown in Scheme 1.

Alekar et al. [55] investigated monovanadium-substituted heteropolymolybdates for catalysis of the hydroxylation of benzene to phenol. They discovered that a vanadium(+5)-peroxo intermediate species was formed during the reactions. Hari Prasad Rao and Ramaswamy also envisaged the formation of a vanadium-peroxo species

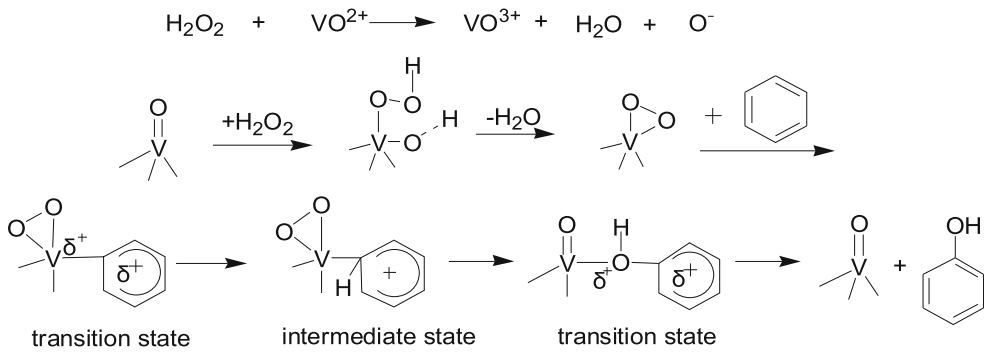

Scheme 1 Proposed mechanism for benzene hydroxylation

by chemisorption of H_2O_2 on isolated vanadium species [56, 57]; the above results are in line with their reports.

4 Conclusion

In summary, mesoporous VO_x/TiO_2 catalysts were prepared by hydrothermal synthesis and were characterized using various instrumental techniques. Vanadium species could be highly dispersed on the mixed-crystal carrier surface at low vanadium contents. When the vanadium loadings was 4.30 wt %, the vanadium species existed in the form of VO_x with two valences, +4 and +5, and the isolated VO_x was highly dispersed on the mixed-crystal carrier surface. The TiV(550)-4.30 catalyst exhibited high catalytic activity for hydroxylation of benzene to phenol. With further increases in the vanadium loading, the high vanadium content resulted in aggregation of vanadium species and formation of a $V_xTi_{1-x}O_2$ rutile-phase solid-solution with TiO_2. This caused changes in the catalyst structure and reduced the amount of active component.

For liquid-phase H_2O_2 hydroxylation of benzene to phenol, the activity of the TiV(550)-4.30 catalyst was higher than those of the other catalysts, and achieved a phenol yield of around 23.8 % and phenol selectivity of about 85 %. XRD, H_2-TPR, and XPS studies showed not only that the VO_x species were highly dispersed, but also that the mixed-crystal carrier interacted strongly with the vanadium species.

Acknowledgments This work was supported by the National Natural Science Foundation of China (21176125), the Science Research Project of the Ministry of Education of Heilongjiang Province of China (2012TD012, 12511Z030, 12521594), and the Graduate Innovation Fund of Heilongjiang Province of China (YJSCX2011-198HLJ, YJSCX2010-024X).

References

1. Hoelderich WF (2000) Appl Catal A Gen 194–195:487
2. Pirutko LV, Chernyavsky VS, Starokon EV, Ivanov AA, Kharitonov AS, Panov GI (2009) Appl Catal B Environ 91:174
3. Liu YY, Murata K, Inaba M (2005) Catal Commun 6:679
4. Bortolotto L, Dittmeyer R (2010) Sep Purif Technol 73:51
5. Chen JQ, Gao S, Xu J (2008) Catal Commun 9:728
6. Feng SJ, Pei SP, Yue B, Ye L, Qian LP, He HY (2009) Catal Lett 131:458
7. Ratnasamy P, Srinivas D, Knözinger H (2004) Adv Catal 48:1
8. Song SQ, Yang HX, Rao RC, Liu HD, Zhang AM (2010) Appl Catal A Gen 375:265
9. Penuka NK (2010) J Mol Catal A: Chem 316:126
10. Liu T, Wei XY, Zhao JJ, Xie HS, Wang TT, Zong ZM (2010) Minist Sci Technol 20:0093
11. Pezhman A, Alireza B, Amir K, Ghodsi MZ (2011) Chin J Catal 32:258
12. Kong Y, Xu XJ, Wu Y, Zhang R, Wang J (2008) Chin J Catal 29:385
13. Qi XY, Li JY, Ji TH, Wang YJ, Feng LL, Zhu YL, Fan XT, Zhang C (2009) Microporous Mesoporous Mater 122:36
14. Zhu YJ, Dong YL, Zhao LN, Yuan FL, Fu HG (2008) Chin J Catal 29:1067
15. Dittmeyer R, Bortolotto L (2011) Appl Catal A Gen 391:311
16. Joseph JK, Singhal S, Jain SL, Sivakumaran R, Kumar B, Sain B (2009) Catal Today 141:211
17. Zhu YJ, Dong YL, Zhao LN, Yuan FL (2010) J Mol Catal A: Chem 315:205
18. Chen JQ, Gao S, Li J, Lv Y (2011) Chin J Catal 32:1446
19. Yin JS, Jia LH, Guo XF, Zhang XJ (2012) Chin J Appl Chem 29:57
20. Mogkhonsi T, Kershenbaum L (1998) Appl Catal A Gen 170:33
21. Bucharsky EC, Schell G, Oberacker R, Hoffmann MJ (2009) J Eur Ceram Soc 29:1955
22. Centi G, Pinelli D, Triforo F, Ghoussoub D, Guelton M, Gengembre L (1991) J Catal 130:238
23. Centi G (1996) Appl Catal A Gen 147:267
24. Narayana KV, Venugopal A, Rao KSR, Masthan SK, Rao VV, Rao PK (1998) Appl Catal A Gen 167:11
25. Chen L, Li JH, Ge MF (2011) Chem Eng J 170:531
26. Casagrande L, Lietti L, Nova I, Forzatti P, Baiker A (1999) Appl Catal B Environ 22:63
27. Reiche MA, Ortelli E, Baiker A (1999) Appl Catal B Environ 23:187
28. Rodella CB, Mastelaro VR (2003) J Phys Chem Sol 64:833
29. Reddy BM, Mehdi S (1993) Reddy EP 20:317
30. Bulushev DA, Kiwi-Minsker L, Zaikovskii VI, Lapina OB, Ivanov AA, Reshetnikov SI, Penken A (2000) Appl Catal A Gen 202:243
31. Martin ST, Morrison CL, Hoffmann MR (1994) J Phys Chem 98:13695
32. Wang YD, Ma CL, Sun XD, Li HD (2003) Appl Catal A Gen 246:161
33. Hongo T, Yamazaki A (2011) Microporous Mesoporous Mater 142:316

34. Du JM, Liu ZM, Li ZH, Han BX, Huang Y, Gao YN (2005) Microporous Mesoporous Mater 83:19
35. Lv CX, Zhou Y, Li H, Dang MM, Guo CC, Ou YC, Xiao B (2011) Appl Surf Sci 257:5104
36. Hausinger G, Schmelz H, Knözinger H (1988) Appl Catal 39:267
37. Yue WB, Xu XX, Irvine JTS, Attidekou PS, Liu C, He HY, Zhao DY, Zhou WZ (2009) Chem Mater 21:2540
38. Kim DS, Han SJ, Kwak SY (2007) J Colloid Interface Sci 316:85
39. Li Q, Yang HS, Qiu FM, Zhang XB (2011) J Hazard Mater 192:915
40. Qian XF, Wan Y, Wen YL, Jia NQ, Li HX, Zhao DY (2008) J Colloid Interface Sci 328:367
41. Zhu CL, Yu HL, Zhang Y, Wang TS, Ouyang QY, Qi LH, Chen YJ, Xue XY (2012) Appl Mater Inter 4:665
42. Adamski A, Sojka Z, Dyrek K, Che M, Wendt G, Albrecht S (1999) Langmuir 15:5733
43. Bond GC (1997) Appl Catal A Gen 157:91
44. Sereda G, Marshall C, Libera JA, Dreessen J, Grady A, Turner M (2012) Catal Lett
45. Nguyen LD, Loridant S, Launay H, Pigamo A, Dubois JL, Millet JMM (2006) J Catal 237:38
46. Kang QM, Yuan BL, Xu JG, Fu ML (2011) Catal Lett 141:1371
47. Silversmit G, Depla D, Poelman H, Marin GB, Gryse RD (2006) Surf Sci 600:3512
48. Bayati MR, Fard FG, Moshfegh AZ (2010) Catal Lett 134:162
49. Tuel A, Taârit YB (1993) Appl Catal A Gen 102:201
50. Molinari R, Lavorato R, Poerio T (2012) Appl Catal A Gen 417–418:87
51. Jian M, Zhu LF, Wang JY, Zhang J, Li GY, Hu CW (2006) J Mol Catal A: Chem 253:1
52. Zhang J, Tang Y, Li GY, Hu CW (2005) J Mol Catal A: Chem 278:251
53. Wang JY, Hu CW, Jian M, Zhang J, Li GY (2006) J Catal 240:23
54. Wang JY, Fu XH, Wang J, Hu CW (2009) Sci China, Ser B: Chem 52:2096
55. Alekar NA, Indira V, Halligudi SB, Srinivas D, Gopinathan S, Gopinathan C (2000) J Mol Catal A: Chem 164:181
56. Hari Prasad Rao PR, Ramaswamy AV, Patnasamy P (1992) J Catal 137:225
57. Hari Prasad Rao PR, Ramaswamy AV (1993) Appl Catal A Gen 93:123